Published in final edited form as:
Adv Mater. 2013 September 14; 25(34): 4707–4713. doi:10.1002/adma.201302025.

Scalable Manufacture of Built-to-Order Nanomedicine: Spray-assisted Layer-by-Layer Functionalization of PRINT® Nanoparticles

Stephen W. Morton,
Koch Institute for Integrative Cancer Research Department of Chemical Engineering Massachusetts Institute of Technology 77 Massachusetts Avenue, Cambridge, MA 02139 (USA)

Kevin P. Herlihy,
University of North Carolina at Chapel Hill 257 Caudill Labs, South Road, Chapel Hill, North Carolina 27514 (USA)

Kevin E. Shopsowitz,
Koch Institute for Integrative Cancer Research Department of Chemical Engineering Massachusetts Institute of Technology 77 Massachusetts Avenue, Cambridge, MA 02139 (USA)

Jason Deng,
Koch Institute for Integrative Cancer Research Department of Chemical Engineering Massachusetts Institute of Technology 77 Massachusetts Avenue, Cambridge, MA 02139 (USA)

Kevin S. Chu,
University of North Carolina at Chapel Hill 257 Caudill Labs, South Road, Chapel Hill, North Carolina 27514 (USA)

Charles J. Bowerman,
University of North Carolina at Chapel Hill 257 Caudill Labs, South Road, Chapel Hill, North Carolina 27514 (USA)

Joseph M. DeSimone[*], and
University of North Carolina at Chapel Hill 257 Caudill Labs, South Road, Chapel Hill, North Carolina 27514 (USA)

Paula T. Hammond[*]
Koch Institute for Integrative Cancer Research Department of Chemical Engineering Massachusetts Institute of Technology 77 Massachusetts Avenue, Cambridge, MA 02139 (USA)

Abstract

Scalable methods, PRINT® particle fabrication and spray-assisted Layer-by-Layer deposition, are combined to generate uniform and functional nanotechnologies with precise control over composition, size, shape, and surface functionality. A modular and tunable approach towards design of built-to-order nanoparticle systems, spray coating on PRINT® particles is demonstrated

[*]Prof. Paula T. Hammond, hammond@mit.edu, Prof. Joseph M. DeSimone, desimone@email.unc.edu.

The authors wish to dedicate this paper to the memory of Officer Sean Collier, for his caring service to the MIT community and for his sacrifice.

to achieve technologies capable of targeted interactions with cancer cells for applications in drug delivery.

Keywords

Core/Shell Nanoparticles; Thin Films; Nanoimprinting

A significant limitation in the design of new nanotechnologies for drug delivery is the balance between efficacy, safety, and scalability – the three major hurdles to streamlined approval towards the clinic and, ultimately, adaptation in the pharmaceutical industry. Oftentimes, these aspects of nanomedicine are competing, and impose challenging design requirements on systems synthesized in the laboratory. Resource-intensive syntheses or purification procedures, limited material yields, and the difficulty of precisely controlling particle size, morphology, and composition for increasingly complex systems are some of the major challenges that continue to prevent the translation of promising technologies away from the bench-top. For this reason, it is highly desirable to conceive of simple, scalable, and highly controlled methodologies for the manufacture of multi-functional nanoparticles that possess the necessary physicochemical characteristics to be clinically relevant.[1]

The surface chemistry of nanoparticles plays a major role in determining their biological properties. However, many of the current methodologies used to modify the surfaces of nanoparticles are inefficient and labor intensive. Layer-by-layer (LbL) polyelectrolyte deposition is an attractive process for incorporating functionality onto the surfaces of nanocarriers to provide improved stability, enhanced cellular uptake, and targeting capabilities.[2-4] Because small molecule drugs and biologics such as nucleic acids can be included in the nanolayers, it also affords the ability to incorporate additional therapeutics that act as synergistic drug combinations[5] on a single nanoscopic platform and in a fashion such that the release of each can be programmed.[6] Although the use of LbL to modify the surfaces of bulk solids has been known for years, only recently has this technology been successfully applied to nanoparticles for medical applications[7] and only in the past couple of years has it been demonstrated that such systems can exhibit extended biodistribution for systemic *in vivo* delivery[2] and tumor-responsive properties[3] in mouse models. A great deal of promise exists for LbL nanoparticle technologies; however, in contrast to LbL deposition onto bulk surfaces (which is highly efficient and can be performed rapidly using automated dip or spray protocols), LbL functionalization of nanoparticles is comparatively slow and inefficient, typically requiring several centrifugal purification steps between the deposition of subsequent polyelectrolyte layers. Given that for drug delivery it is often desirable to test different surface functionalities and drug combinations, it would be of great interest to develop an LbL platform for NP functionalization that takes advantage of the high throughput and efficiency of more recently developed rapid LbL techniques.

Particle fabrication using the Particle Replication in Non-wetting Templates (PRINT®) process is a well-established, scalable approach[8] for rapidly manufacturing particles with exquisite control over particle geometry (size, shape) and composition (cargo, carrier system), important parameters for optimizing cellular engagement and *in vivo*

pharmacokinetics.[8-10] Through a roll-to-roll process, an elastomeric mold is implemented in a high-throughput fashion to generate monodisperse particles with well-defined geometries. By varying the properties of the elastomeric mold, particles can be produced with a dynamic range of shapes and sizes, varying from 10 nm - 200 μm. Further, particles prior to recovery are presented in an ideal, ordered spatial arrangement that presents an attractive opportunity for high-throughput surface functionalization methodologies, such as LbL. The ability to fabricate precisely controlled nanotechnologies on a large scale is highly attractive towards expedient approval through regulatory pathways.[11]

Purification and surface functionalization of PRINT® particles, however, endures all of the challenges faced by other synthesis techniques. Following particle fabrication, purification from the solubilized transfer adhesive film is limited by traditional means (e.g. ultracentrifugation, tangential-flow filtration). Post-purification modification is generally required to achieve effective surface modification using the more traditional techniques available to the biomaterials community at-large for yielding functional particle systems. Oftentimes, these bioconjugation or functionalization chemistries are difficult and expensive to scale and result in significant material loss. The ability to control surface characteristics is essential to improve performance of nanotechnologies regarding enhanced specific molecular interactions with target cells, as well as avoid non-specific clearance *in vivo* via protein-resistive properties.[12] Surfaces largely mediate interactions at the interface of biology; therefore, the desire to incorporate a technology with the ability to include a library of materials on the surface of PRINT® particles in an analogous high throughput, scalable fashion is highly desirable, and one that holds much promise for the future of multi-functional nanotechnology manufacture.

Towards the development of a complementary, scalable approach for the surface functionalization of roll-to-roll assembled functional nanoparticles, we demonstrate that spray-assisted Layer-by-Layer (Spray-LbL) deposition may be used to generate highly-controlled functional coatings in a rapid, reproducible, and facile manner on a generalizable platform of particle systems, as illustrated in Scheme 1. Spray-LbL has been shown[13] to conformally coat materials on the nanoscale in a controllable fashion, with extremely thin layers deposited on the surface of various charged substrate materials, including 3D structures such as electrospun mats. The combination of PRINT® and LbL technologies offers an expansive toolbox for producing functional particles for a variety of applications, including catalysis, microelectronics, photovoltaics, and cosmetics, in addition to nanomedicine.[14] Bringing PRINT® technology and Spray-LbL functionalization together, this work demonstrates a scalable, reproducible approach for fabrication of functional carriers with exquisite control over particle composition, geometry, and surface properties, providing an exciting platform for large-scale manufacture of highly-controlled multi-functional nanocarriers.

Using the widely-reported top-down approach of PRINT® particle fabrication, 200×200×200nm PLGA nanoparticles ($PLGA_{200\times200nm}$) were fabricated and collected on a low molecular weight polyvinyl alcohol (PVA) base coating atop a polyester support film. While immobilized on the support film, the particles are arranged in a highly ordered 2-D hexagonal array. The PVA supported particles were visualized by AFM and SEM. The

regular spatial arrangement of PRINT® particles coupled with the negative surface charge of the acid-terminated PLGA NPs in water make them ideal candidates for rapid LbL polyelectrolyte functionalization through spray-assisted LbL deposition (Spray-LbL). Initial attempts to deposit aqueous solutions of polyelectrolytes onto the supported PRINT particles resulted in a loss of the particles due to detachment from the substrate. This process could be visualized by the loss of diffraction-based iridescence characteristic of the ordered nanoparticle arrays (Figure 1B, 1C); this characteristic iridescence is indicative of highly ordered particles on the harvesting layer, allowing for a convenient qualitative assessment of particle immobilization or detachment. The loss of particles was confirmed with AFM and SEM, which essentially show a complete absence of particles after the Spray-LbL process due to the water solubility of the PVA backing. The reason for choosing PVA as the support material for PRINT particles is in fact to enable facile particle harvesting (see Supplemental Figure 1).

To avoid PVA dissolution, vapor-phase crosslinking using concentrated glutaraldehyde and acid was employed to selectively crosslink the PVA adhesion layer to reduce its water solubility, while avoiding any chemical changes to the relatively impermeable and inert PLGA PRINT® nanoparticles. Contact angle measurements were carried out to study the effects of the vapor-phase cross-linking reaction on the wettability of the PRINT® films. As shown in the Figure 1A, pre-crosslinked NP arrays show considerable wettability, owing to the presence of highly water-soluble and hydrophilic PVA polymer. After cross-linking, the contact angle increased from 26° to 78° (Figure 1D), demonstrating that the films become considerably more hydrophobic due to the formation of a glutaraldehyde cross-linked PVA adhesive. Crosslinking conditions were also varied with results shown in Supplemental Figure 2. As a result, the cross-linked films can be placed in water without particle detachment. Following crosslinking, it was observed that particles could be readily functionalized, as evidenced by maintenance of iridescence from the NP array following each processing step (Figure 1E, 1F). This step therefore allowed for the deposition of water-based polyelectrolytes using Spray-LbL.

As shown in Scheme 1, Spray-LbL on PRINT® nanoparticles, following vapor-phase cross-linking of the PVA support films, is achieved by spraying an aqueous solution of cationic polyelectrolyte is sprayed onto the NP containing films for 3 seconds and, after briefly rinsing with water (3 seconds), an anionic polyelectrolyte is subsequently sprayed onto the films (3 seconds). This cycle can then be repeated indefinitely to control the thickness of the polyelectrolyte coating. In the final step, the particles are harvested by sonicating the films in water, which causes the particles to detach from the PVA substrate.

Using AFM, the shape, persistence and uniformity of the particles were monitored with each processing step, beginning with the initial NP array, followed by crosslinking, and subsequent Spray-LbL deposition, as shown in Figure 2 (corresponding amplitude images shown in Supplemental Figure 3). The versatility of this platform was further demonstrated by coating a second PRINT® PLGA particle type, 80×80×320nm [$PLGA_{80\times320nm}$]. AFM confirms that the particles are coated in a manner that maintains the uniformity of the PRINT® particle template while building a film, observed by slight increase in height

(~5nm/bilayer), which avoids bridging of neighboring particles and without causing significant loss of particles during functionalization.

Particles were subsequently recovered via sonication, purified via filtration, and concentrated using ultracentrifugation following Spray-LbL. A variety of techniques were then used to illustrate the uniformity of the particles obtained from this fabrication method. Dynamic light scattering analysis is shown in Table 1, with the corresponding histograms shown in Supplemental Figure 4. For both particle types, uniformity of the particle population is maintained as evidenced by the PDI of functionalized particles (see Table 1: PRINT® $PLGA_{200\times200nm}$ particles - original 0.01, 0.06 following deposition of three bilayers of PLL/HA_{500K}; PRINT® PLGA80×320nm particles – original 0.05). A slight decrease in size following crosslinking is observed for both particle types, consistent with the amount of material exposure to the crosslinking contraction forces on the PVA adhesive layer. The change in size for functionalized particles is indicative of a very thin LbL film, approximately 15-20nm for 3 bilayers of PLL/HA_{500K}, based on dynamic light scattering (Table 1) and confirmed with electron microscopy (Figures 3, 4). Histogram overlays also illustrate the thin coatings applied to the particle surface (Supplemental Figure 4). Characteristic surface charge reversal of the LbL deposition is also observed, as evidenced by samples taken at different steps in the functionalization process. ζ-potential, measured at 25°C in 10mM NaCl, of pre- and post-XL NPs are approximately the same, while deposition of materials post-XL results in surface charge characteristics consistent with the material deposited (see Supplemental Figure 4). A range of polyelectrolyte multilayers were explored, including poly-L-lysine (PLL)/hyaluronic acid (HA) [PLL/HA_{500K}], PLL/dextran sulfate (DXS) [PLL/DXS], PLL/poly(acrylic acid) [PLL/PAA], chitosan/HA [Chit/HA_{500K}], and chitosan/PAA [Chit/PAA] (see Supplemental Figure 4), further illustrating a primary advantage of LbL as a means of tailoring the surface properties of these NP systems. These films, while diverse in the range of materials incorporated, behaved similarly in coating the NP systems without compromising the particle shape or significantly increasing the size beyond a few tens of nanometers.

Recovered and purified particles visualized by electron microscopy, including SEM and TEM, are displayed in Figures 3 and 4. Figures 3A and 3B are representative of the uncoated, crosslinked PRINT® $PLGA_{200\times200nm}$ particle array, along with the corresponding recovered particles observed by both SEM (Figure 3C) and TEM (Figure 4B). The coated array is shown in Figure 3D and 3E for direct comparison. A thin film coating is observed on the particles in such a fashion that individual particle integrity is maintained prior to recovery. Subsequent recovery yields the results in Figure 3F, where a thin coating of approximately 20nm is observed to surround the entire particle surface by TEM (Figure 4B). Observation of a conformal coating surrounding the entire nanoparticle is a surprising result due to the inaccessibility of the spray deposition to the immobilized surface; however, it can be explained by the unique feature of the electrostatic self-assembly LbL process to “self-heal” defects in the adsorbed film.[15] The excess film that corrects for this defect in spray LbL on PRINT® is observed in Figure 3E, whereby the film surrounding the individual nanoparticle collapses in a manner that completely and smoothly seals the nanoparticle with deposited film around the harvested particle following suspension. This phenomenon is also observed for the $PLGA_{80nm\times320nm}$ NPs. Displayed in Figure 3G and 3H are the uncoated,

crosslinked $PLGA_{80\times320nm}$ NP arrays, followed by the recovered particles visualized by both SEM (Figure 3I) and TEM (Figure 4E). Compared to the coated NP arrays in Figure 3J and 3K, the particles clearly grow in size in both dimensions following film deposition. This thin film is also observed following recovery in using both SEM (Figure 3L) and TEM (Figure 4E), where a coating of 20nm is observed around the entire particle. From these data, it is clear that we can conformally coat PRINT® PLGA NPs with films around the entire particle surface and in a manner that preserves the monodispersity of the platform.

After demonstrating the feasibility of spray functionalization and observing a conformal coating surrounding two different PRINT® NP templates with a variety of coating materials, it was important to examine the ability to control film growth using Spray-LbL. Control over film thickness will allow precise tuning of drug release for therapeutic-containing NP systems as well as functionalization of these material systems in such a way that does not significantly impact the NP size or shape, which is a primary advantage of PRINT® manufacture. From Figures 3, 4B, 4E, it was observed that three bilayers of PLL/HA (3 seconds/spray) generate a film of approximately 15nm. To observe whether thicker films could be generated, high molecular weight polymers (Chitosan, 200K; HA, 500K) were sprayed (3 seconds/spray) alternately to yield a 5 bilayer film. As expected, this film was found to be significantly thicker, approximately 40nm by TEM (Figure 4C, 4F), while conformally coating the NP surface so as to not compromise the NP shape. SEMs of the coated backings and subsequent harvested and purified coated NPs for each PRINT® template are displayed in Supplemental Figure 5. TEMs of each corresponding uncoated NP systems are displayed in Figure 4A and 4D for reference. This effectively demonstrates the capability of Spray-LbL as a means of tuning film thickness by incorporating higher molecular weight polymers with more bilayer coatings. Additional parameters to tune film thickness are longer spray times and higher concentrations of material sprayed.

As an additional test of particle functionalization, the polycationic layer, poly-L-lysine (PLL), was labeled with a Cy5.5 dye (Lumiprobe, Cy5.5-NHS ester). Deposition was tracked using fluorescence imaging and shown to significantly increase following layers 1 and 3, consistent with the subsequent addition of $PLL_{Cy5.5}$. This is also demonstrated by directly comparing PLL/DXS films cast both with and without PLLCy5.5 using confocal microscopy (Supplemental Figure 6).

While particle functionalization is clearly demonstrated and in a reproducible manner, questions regarding biological functionality remained as this component of the carrier system is critical to the translational relevance of the technology. Using the labeled $PLL_{Cy5.5}$ Spray-LbL functionalized NP systems, particles were incubated with a triple negative breast cancer cell line, BT-20. These cells, like many aggressive cancer cell types, characteristically overexpress CD44 receptors[16], which are a convenient target for the natural ligand, hyaluronic acid.[17] Previous work has also shown much promise for HA-coated systems to provide a serum-stable, stealth-like platform for delivery.[2] Investigations of cell-associated fluorescence in combination with confocal microscopy, shown in Figure 5A-5D, confirmed that these coatings are functional, as shown with enhanced levels of cell uptake for the HA-coated systems. Further, increased uptake for HA-coated systems is clear relative to the non-specific uptake of the DXS-terminated system, suggesting that film

construction can be finely tuned towards targeting specific cell populations. In this way, Spray-LbL on PRINT® presents exciting opportunities to not only functionalize particles scalably, reproducibly, and with extremely thin coatings but also in a manner that molecular engagement of target cells can be achieved.

Particle shape also plays a significant role in cellular internalization, as shown in Figure 5E-5G. Coated $PLGA_{80\times320nm}$ NPs ($[PLL/HA]_3$) exhibited nearly 10-fold higher levels of cell association relative to identically-coated $PLGA_{200\times200nm}$ NPs within 2h of treatment, as determined by FACS. This enhanced level of uptake is further complemented by confocal microscopy, from which significantly more punctate NP fluorescence is observed inside the cells for the $PLGA_{80\times320nm}$ NPs. The impact of particle size and shape on cellular internalization is of particular interest towards designing effective carrier systems that further mediate endocytosis, in addition to surface chemical functionality. This proves highly promising towards combination of optimal PRINT® technologies with target-specific Spray-LbL architectures to maximize therapeutic impact of these NP systems.

Spray-LbL on PRINT® is a significant advance in the design of nanotechnology, as it provides an exciting platform for large-scale production of built-to-order functional nanoparticle systems, whereby we have precise control of the physicochemical characteristics of the NP systems developed. This includes the ability to finely tune the NP shape, size, chemical composition, and surface characteristics towards manufacture of systems that maximize cellular entry and optimize drug and NP pharmacokinetics *in vivo*. Further, the ability to rapidly and scalably manufacture these systems is realizable, as PRINT® technology is capable of roll-to-roll NP fabrication while spray can be applied in a continuous fashion. This compatibility in continuous manufacture and subsequent functionalization of NP systems presents a highly attractive opportunity for highly reproducible manufacture of customizable NP systems for a wide variety of applications.

Experimental

All materials and equipment necessary for PRINT® particle fabrication were maintained in a clean room under controlled conditions at UNC-Chapel Hill. Bulk material, including rolls of poly(ethylene terephthalate) [PET], poly(vinyl alcohol) [PVA]-coated PET, and pre-made molds cast from a perfluoropolyether (PFPE) material, were provided by Liquidia Technologies. All chemicals used were provided by Sigma Aldrich, except for hyaluronic acid, provided by Lifecore Biomedical, and Cy5.5-NHS from Lumiprobe.

PRINT® Nanoparticle Fabrication

PRINT® particle fabrication follows a well-established protocol.[9] Briefly, the polymeric material, poly(lactide co-glycolic acid) [PLGA], used for particle molding was dissolved in dichloromethane. A film of PLGA was cast using a mayer rod (#3) on a high energy PET backing prior to lamination of this film to the pre-cast mold at 320°F. The filled mold from this step was laminated at 320°F to a transfer adhesive film (PVA) cast on a PET backing. The particles were preserved in this state via vacuum seal under N_2 atmosphere until ready for functionalization.

Vapor-phase Glutaraldehyde Crosslinking

Molded nanoparticles were delaminated from the mold onto the transfer adhesive film. Sections of these harvested particles were subjected to PVA-crosslinking conditions in an enclosed chamber via vapor-phase glutaraldehyde crosslinking to further immobilize the particles for spray-LbL deposition. This was done via incubation of the particle arrays with vials containing 50% glutaraldehyde (in water) and 10% aqueous acid (HCl) for 15h. Arrays following crosslinking were removed for subsequent functionalization.

Spray Layer-by-Layer Deposition

Materials were deposited onto the surface of crosslinked nanoparticle arrays by aerosolization of polyelectrolytes for spray times of ~3 seconds, with ~3 second wash steps between each layer. Polyelectrolytes were sprayed at a concentration of 1mg/mL. A final water rinse was used prior to drying and subsequent analysis and/or recovery of functionalized particles. Particles recovered following spray-LbL were harvested by sonication of the functionalized particle arrays in water for ~15minutes. The collected particles were subsequently purified via centrifugation and filtration through a 0.45μm syringe filter.

Nanoparticle Characterization

Images to assess iridescence of the nanoparticle arrays following each processing step were obtained by photography with a 5-megapixel camera (iPhone 4). Contact angle measurements and images (Rame-Hart model 500 goniometer with Nikon camera) were obtained immediately following drop-casting a bubble of water on the NP array. Dynamic light scattering (Malvern ZS90) was used to determine the hydrodynamic diameter of the nanoparticles. Zeta potential measurements were also performed using the Malvern ZS90. Measurements were conducted in 10mM NaCl in millipore water at 25°C.

Scanning electron micrographs were collected using a JEOL 6700 high resolution microscope. Sample preparation included drop-casting on a silicon wafer followed by sputter coating with gold-palladium (~3nm). Transmission electron micrographs were collected using a JEOL 2010 Advanced High Performance TEM. Sample preparation included drop-casting on a carbon/formvar-coated copper grid. Atomic force microscopy data was collected using a MultiMode™ atomic force microscope with a NSC15/AIBS, 325kHz, 46N/m tip from μmasch in tapping mode.

Confocal microscopy (Nikon A1R scanning confocal microscope) was conducted following incubation of the functionalized nanoparticles (tracked via labeled PLL, $PLL_{Cy5.5}$) at 37°C with BT-20 cells. Fixed samples included a DAPI and Phalloidin-488 stain, in addition to particle tracking Cy5.5 label. Flow cytometry (BD LSRFortessa) was performed in parallel with confocal microscopy to quantitatively assess particle association (tracking via $PLL_{Cy5.5}$) with cells following incubation at 37°C. Particles administered were normalized against the fluorescent intensity (λ_{ex}=675nm, λ_{em} = 710nm), as measured by a Tecan Microplate Reader, of the labeled polycationic layer deposited initially on the NP surface.

Supplementary Material

Refer to Web version on PubMed Central for supplementary material.

Acknowledgments

The authors would like to thank funding for providing valuable resources to facilitate this work. These include grants from the Center for Cancer Nanotechnology Excellence (CCNE), grant numbers: 5 U54 CA151884-02 (MIT), U54CA151652 (UNC). The authors would also like to acknowledge Liquidia Technologies for providing materials to support this work, as well as the Koch Institute for Integrative Cancer Research at MIT for providing access to resources central to the completion of this work. The authors would further like to thank Bill DiNitale and Institute for Soldier Nanotechnologies, Center for Materials Science and Engineering (CMSE) at MIT, and Chapel Hill Analytical and Nanofabrication Laboratory (CHANL) for assistance and facilities supporting electron microscopy work. Finally, the authors would like to thank the Koch Institute Swanson Biotechnology Center core facilities (microscopy, flow cytometry) for facilitating biological data. S.W.M. would like to acknowledge funding from the National Science Foundation Graduate Research Fellowship (N.S.F. G.R.F.P.). K.E.S. would like to acknowledge National Sciences and Engineering Research Council (N.S.E.R.C.) for a postdoctoral fellowship.

References

[1]. Peer D, Karp JM, Hong S, FaroKhzad OC, Margalit R, Langer R. Nat. Nanotechnol. 2007; 2:751. [PubMed: 18654426] Shi JJ, Xiao ZY, Kamaly N, Farokhzad OC. Accounts Chem. Res. 2011; 44:1123.Wei A, Mehtala JG, Patri AK. Journal of Controlled Release. 2012; 164:236. [PubMed: 23064314]

[2]. Poon Z, Lee JB, Morton SW, Hammond PT. Nano Lett. 2011; 11:2096. [PubMed: 21524115]

[3]. Poon Z, Chang D, Zhao X, Hammond PT. ACS Nano. 2011; 5:4284. [PubMed: 21513353]

[4]. Hammond PT. Materials Today. 2012; 15:196.Hammond PT. Nanomedicine. 2012; 7:619. [PubMed: 22630144] Morton SW, Poon Z, Hammond PT. Biomaterials. 2013; 34:5328. [PubMed: 23618629]

[5]. Lee, Michael J.; Ye, Albert S.; Gardino, Alexandra K.; Heijink, Anne M.; Sorger, Peter K.; MacBeath, G.; Yaffe, Michael B. Cell. 2012; 149:780. [PubMed: 22579283] Lehar J, Krueger AS, Avery W, Heilbut AM, Johansen LM, Price ER, Rickles RJ, Short GF Iii, Staunton JE, Jin X, Lee MS, Zimmermann GR, Borisy AA. Nat Biotech. 2009; 27:659.

[6]. Shukla A, Fuller RC, Hammond PT. Journal of Controlled Release. 2011; 155:159. [PubMed: 21699932] Smith RC, Riollano M, Leung A, Hammond PT. Angewandte Chemie International Edition. 2009; 48:8974.

[7]. Gittins DI, Caruso F. Advanced Materials. 2000; 12:1947.Lvov YM, Pattekari P, Zhang X, Torchilin V. Langmuir. 2010; 27:1212. [PubMed: 21190345] Schneider, G. g. F.; Subr, V.; Ulbrich, K.; Decher, G. Nano Letters. 2009; 9:636. [PubMed: 19170551] Cortez C, Tomaskovic-Crook E, Johnston APR, Scott AM, Nice EC, Heath JK, Caruso F. ACS Nano. 2007; 1:93. [PubMed: 19206525]

[8]. Canelas DA, Herlihy KP, DeSimone JM. Wiley Interdisciplinary Reviews: Nanomedicine and Nanobiotechnology. 2009; 1:391. [PubMed: 20049805]

[9]. Perry JL, Herlihy KP, Napier ME, DeSimone JM. Accounts Chem. Res. 2011; 44:990.

[10]. Merkel TJ, Herlihy KP, Nunes J, Orgel RM, Rolland JP, DeSimone JM. Langmuir. 2009; 26:13086. [PubMed: 20000620] Zhang H, Nunes JK. New J. Phys. 2009; 11:075018.Gratton SEA, Ropp PA, Pohlhaus PD, Luft JC, Madden VJ, Napier ME, DeSimone JM. Proceedings of the National Academy of Sciences of the United States of America. 2008; 105:11613. [PubMed: 18697944]

[11]. Gaspar R, Duncan R. Advanced Drug Delivery Reviews. 2009; 61:1220. [PubMed: 19682513] Duncan R, Gaspar R. Molecular Pharmaceutics. 2011; 8:2101. [PubMed: 21974749]

[12]. Owens DE Iii, Peppas NA. International Journal of Pharmaceutics. 2006; 307:93. [PubMed: 16303268]

[13]. Krogman KC, Lowery JL, Zacharia NS, Rutledge GC, Hammond PT. Nat Mater. 2009; 8:512. [PubMed: 19377464] Krogman KC, Zacharia NS, Schroeder S, Hammond PT. Langmuir. 2007; 23:3137. [PubMed: 17288468]

[14]. Zhang L, Gu FX, Chan JM, Wang AZ, Langer RS, Farokhzad OC. Clin Pharmacol Ther. 2007; 83:761. [PubMed: 17957183] Davis ME, Chen Z, Shin DM. Nat Rev Drug Discov. 2008; 7:771. [PubMed: 18758474]

[15]. Bertrand P, Jonas A, Laschewsky A, Legras R. Macromolecular Rapid Communications. 2000; 21:319.

[16]. Platt VM, Szoka FC. Molecular Pharmaceutics. 2008; 5:474. [PubMed: 18547053]

[17]. Hyung W, Ko H, Park J, Lim E, Park SB, Park Y-J, Yoon HG, Suh JS, Haam S, Huh Y-M. Biotechnology and Bioengineering. 2008; 99:442. [PubMed: 17625788] Luo Y, Ziebell MR, Prestwich GD. Biomacromolecules. 2000; 1:208. [PubMed: 11710102] Surace C, Arpicco S, Dufaÿ-Wojcicki A. l. Marsaud V. r. Bouclier C. l. Clay D, Cattel L, Renoir J-M, Fattal E. Molecular Pharmaceutics. 2009; 6:1062. [PubMed: 19413341] Eliaz RE, Szoka FC. Cancer Research. 2001; 61:2592. [PubMed: 11289136]

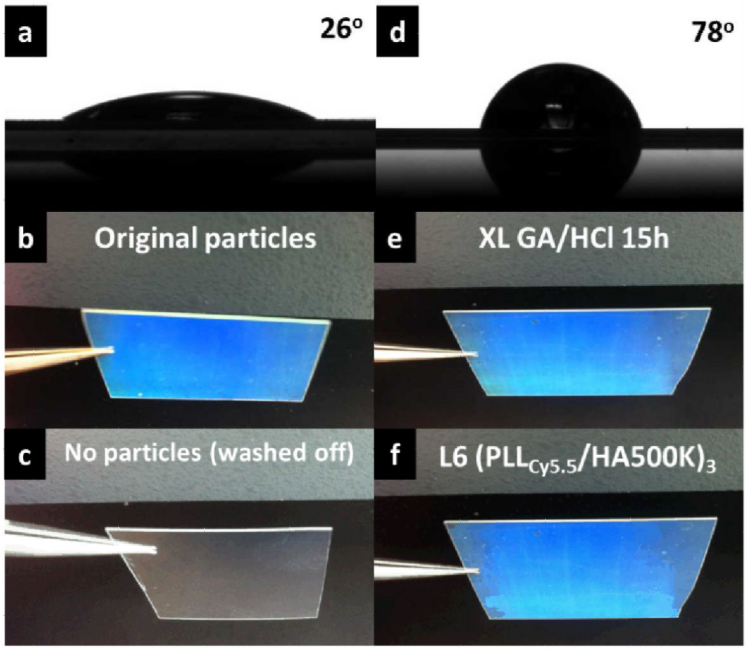

Figure 1. Contact angle and particle iridescence characterization pre- and post-functionalization

(a) Contact angle measurement and image of pre-crosslinked NP array. **(b)** Particle iridescence observed in the ordered particle array post-PRINT® fabrication. **(c)** Loss of iridescence following spray of water-based polyelectrolytes, indicative of complete loss of particles. **(d)** Contact angle measurement and image of post-crosslinked NP array (glutaraldehyde/HCl vapor phase crosslinking). Particle iridescence is maintained following **(d)** 15h crosslinking and **(f)** Spray-LbL deposition of $[PLL/HA]_3$.

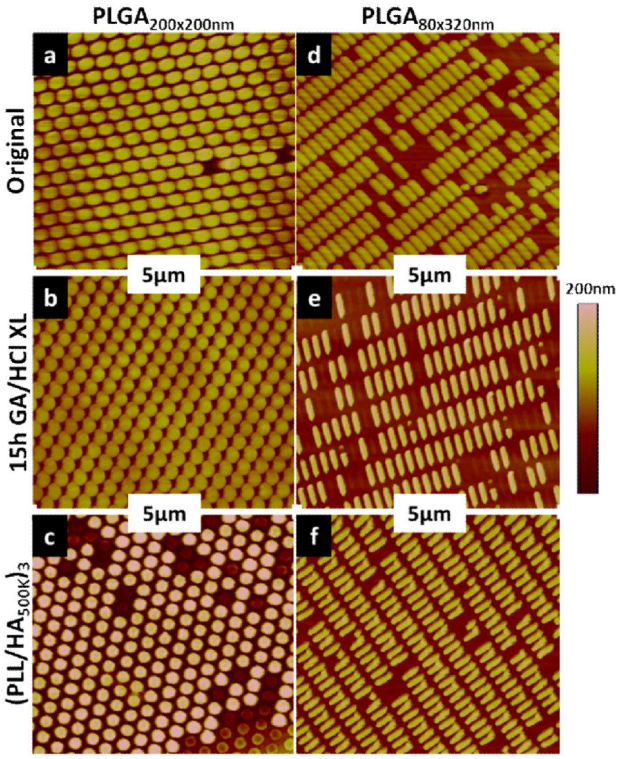

Figure 2. AFM characterization of nanoparticle arrays - height

(a) Pre-crosslinked $PLGA_{200\times200nm}$ NP array; (b) $PLGA_{200\times200nm}$ NP array following crosslinking; (c) $PLGA_{200\times200nm}/(PLL/HA_{500K})_3$. (d) Pre-crosslinked $PLGA_{80\times320nm}$ NP array; (e) $PLGA_{80\times320nm}$ NP array following crosslinking; (f) $PLGA_{80\times320nm}/(PLL/HA_{500K})_3$. Scale bars representative of 2μm. Color scale representative of linear gradient from 0 [bottom] to 200 nm [top].

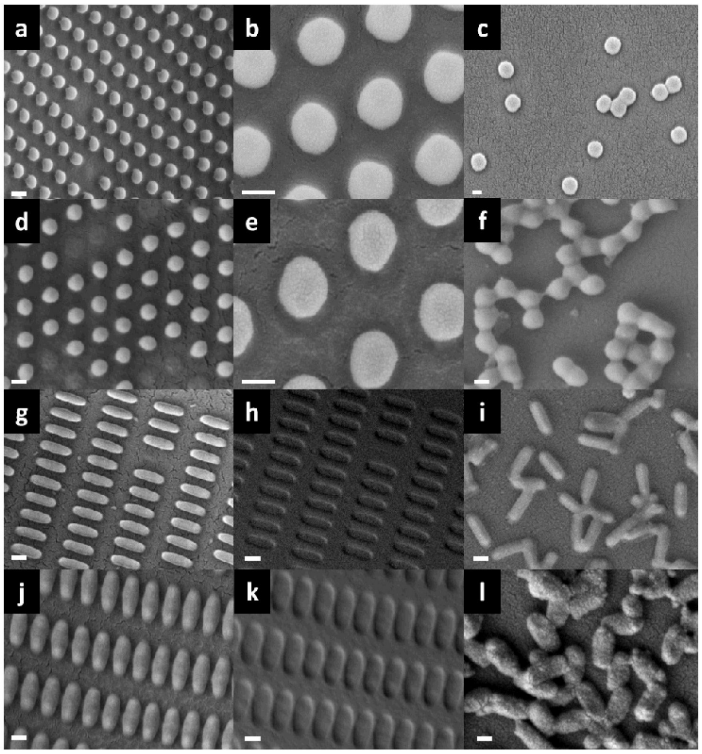

Figure 3. SEM characterization of particles pre- and post-Spray-LbL functionalization

SEM of **(a,b)** uncoated, crosslinked 200×200nm PLGA NP array; **(c)** purified uncoated, crosslinked 200×200nm PLGA NPs; **(d,e)** coated 200×200nm PLGA NP array [(PLL/HA)$_3$]; **(f)** purified coated 200×200nm PLGA NPs [(PLL/HA)$_3$; **(g,h)** uncoated, crosslinked 80×320nm PLGA NP array; **(i)** purified uncoated, crosslinked 80×320nm PLGA NPs; **(j,k)** coated 80×320nm PLGA NP array [(PLL/HA)$_3$]; **(l)** purified coated 80×320nm PLGA NPs [(PLL/HA)$_3$]. Scale bars representative of 200nm.

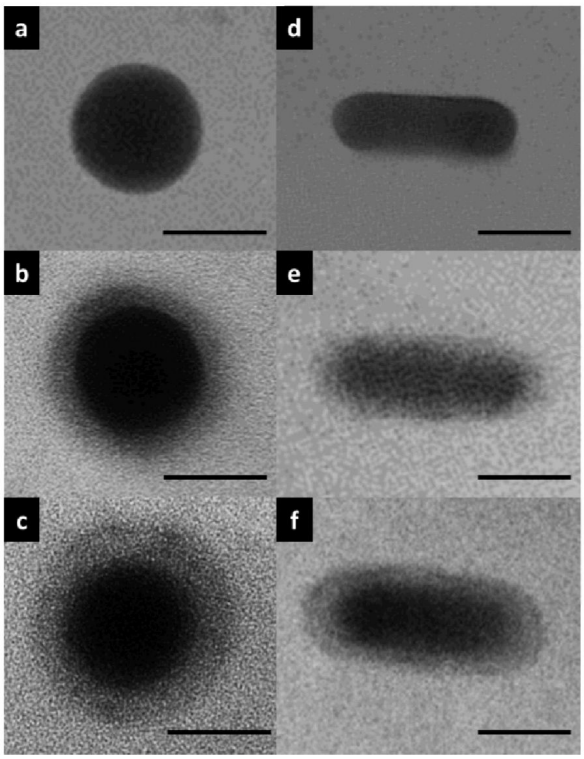

Figure 4. TEM characterization of particles pre- and post-Spray-LbL functionalization - controlling film thickness

TEM of (a) uncoated, crosslinked 200×200nm PLGA NPs; (b) purified coated 200×200nm PLGA NPs [$(PLL/HA)_3$]; (c) purified coated 200×200nm PLGA NPs [$(Chit/HA)_5$]; (d) uncoated, crosslinked 80×320nm PLGA NPs; (e) purified coated 80×320nm PLGA NPs [$(PLL/HA)_3$]; (f) purified coated 80×320nm PLGA NPs [$(Chit/HA)_5$]. Scale bars representative of 100nm. TEMs of uncoated, uncrosslinked NPs are displayed in Supplemental Figure 10.

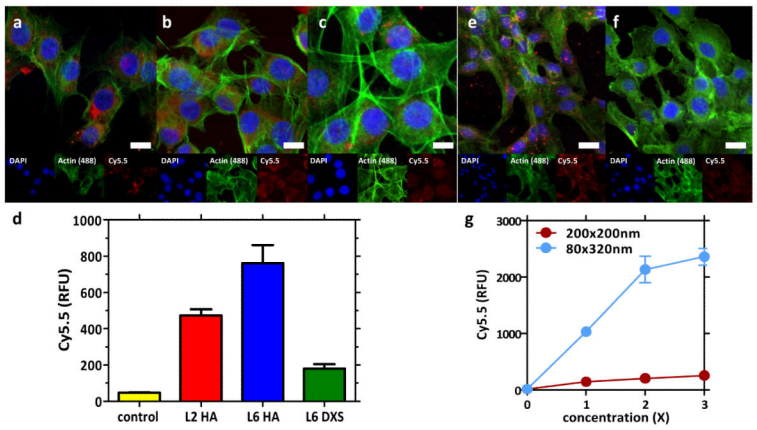

Figure 5. Confocal microscopy and cell-associated fluorescence of Spray-LbL PRINT® particles via tracking with $PLL_{Cy5.5}$ polycationic component – investigation of variable coatings, coating thickness, and NP shape

Confocal microscopy of (a) $PLGA_{200\times200nm}$/PLL/HA_{500K} NPs [L2 HA], (b) $PLGA_{200\times200nm}$/(PLL/HA_{500K})$_3$ NPs [L6 HA], (c) $PLGA_{200\times200nm}$/PLL/DXS NPs [L6 DXS] incubated with BT-20 cells for 6h at 37°C. NPs labeled with $PLL_{Cy5.5}$ as first polycationic component in film and normalized in dose based on the absorbance of this layer on the functionalized NPs. (d) Mean cell-associated fluorescence [Cy5.5 channel (λ_{ex} = 640nm, λ_{em} = 700nm)] for each NP formulation displayed in (a)-(c). Data presented as the average +/− SEM of triplicate measurements. Confocal microscopy of (e) $PLGA_{80\times320nm}$/(PLL/HA_{500K})$_3$ NPs and (f) $PLGA_{200\times200nm}$/(PLL/HA_{500K})$_3$ NPs incubated with BT-20 cells for 2h at 37°C. NPs labeled with $PLL_{Cy5.5}$ as first polycationic component in film and normalized in dose based on the absorbance of this layer on the functionalized NPs. (g) Mean cell-associated fluorescence [Cy5.5 channel (λ_{ex} = 640nm, λ_{em} = 700nm)] for each NP formulation displayed in (e)-(f). Data presented as average +/− SEM of triplicate measurements. Confocal microscopy images representative of overlays of individual fluorescence channels displayed below [from left to right under each overlay: DAPI nuclear stain, phalloidin-488 stain, NP fluorescence – Cy5.5].

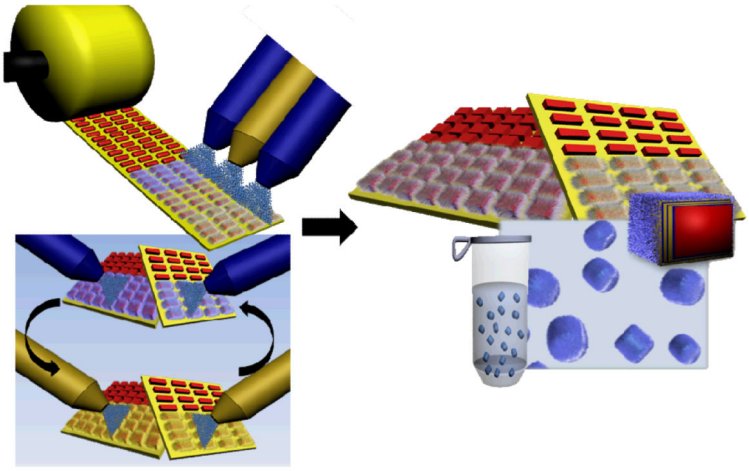

Scheme 1. Spray-LbL on PRINT® nanoparticles

PRINT® particles were fabricated and used while immobilized in a post-harvesting array for Spray-LbL. Arrays were subsequently crosslinked under vapor-phase glutaraldehyde/concentrated acid conditions, followed by LbL application (sequential deposition of polycation/wash/polyanion/wash comprising one bilayer). Functionalized particles were harvested by sonication of the arrays in water and purified by filtration and ultracentrifugation.

Table 1

Nanoparticle physicochemical characterization

Dynamic light scattering data, based on z-average hydrodynamic diameter, and zeta-potential measurements were conducted at 25°C in 10mM NaCl/deionized water. Data is presented for purified, uncoated $PLGA_{200\times200nm}$ and $PLGA_{80\times320nm}$ NPs, purified $PLGA_{200\times200nm}$ and $PLGA_{80\times320nm}$ following crosslinking, and coated NPs: $PLGA_{200\times200nm}/(PLL/HA_{500K})_3$ and $PLGA_{80\times320nm}/(PLL/HA_{500K})_3$. Data for mean hydrodynamic diameter and zeta-potential are presented as average +/− standard error of the mean for triplicate measurements.

Spray-LbL on PRINT®	**$PLGA_{200\times200nm}$**	**$PLGA_{200\times200nm}$ XL**	**$PLGA_{200\times200nm}/(PLL/HA)_3$**	**$PLGA_{80\times320nm}$**	**$PLGA_{80\times320nm}$ XL**	**$PLGA_{80\times320nm}/(PLL/HA)_3$**
Mean d_h [nm] +/− SEM	237 +/− 2	229 +/− 3	244 +/− 2	221 +/− 1	192 +/− 2	214 +/− 5
PDI	0.01	0.03	0.06	0.06	0.1	0.05
ζ potential [mV] +/− SEM	−6 +/− 0.1	−8 +/− 2	−28 +/− 1	−10 +/− 2	−13 +/− 0.5	−24 +/− 2